# A STUDY ON THE FLOW PATTERNS OF A SECOND GRADE VISCOELASTIC FLUID PAST A CAVITY IN A HORIZONTAL CHANNEL

**C. H. Hsu S. Y. Hu**

*Department of Mechanical Engineering*
*Chung-Yuan Christian University*
*Taoyuan, Taiwan 32023, R.O.C.*

**C. C. Kuo** *

*Department of Mechanical Engineering*
*Taoyuan Innovation of Institute Technology*
*Chung Li, Taiwan 32091, R.O.C.*

**K. Y. Kung**

*Graduate School of Materials Applied Technology*
*Taoyuan Innovation of Institute Technology*
*Taoyuan, Taiwan 32091, R.O.C.*

**C. C. Chang**

*Department of Mechanical Engineering*
*Army Academy R.O.C*
*Taoyuan, Taiwan 32093, R.O.C.*

**ABSTRACT**

This paper studies the behavior of second grade viscoelastic fluid past a cavity in a horizontal channel. The effects of Reynolds number, fluid elasticity and the aspect ratio of the cavity on the flow field are simulated numerically. The equations are converted into the vorticity and stream function equations. The solution is obtained by the finite difference method.

The behavior of viscoelastic fluids is quite different from the Newtonian fluid, due to the effects of fluid elasticity. Only one flow pattern appears when the Newtonian fluid past the cavity. However, three kinds of flow patterns appear while the viscoelastic fluids past the cavity by increasing Reynolds number from 20 to 300. The flow field is affected by the fluid elasticity as well as the aspect ratio of the cavity. The transitional flow pattern appears at lower Reynolds number as the higher elasticity fluid past the cavity with larger aspect ratio.

**Keywords:** Cavity, Elastic coefficient, Horizontal channel, Reynolds number, Viscoelastic fluid.

## 1. INTRODUCTION

Many researches about the viscoelastic fluid and cavity flow were reported in the past decade. The flow of a viscoelastic fluid past a cavity is considered to be more complex than the Taylor – Couette and Dean flow (Grillet, Shaqfeh *et al.* [1]). The viscoelastic fluid, a kind of non-Newtonian fluid, has both viscosity and elasticity characteristics. Because of its elasticity characteristics, the flow phenomena of viscoelastic fluid flow are significantly different from that of the Newtonian fluid flow, *e.g.* the secondary recirculation zone and reattachment length (Hsu and Chou [2]).

Many complex flow phenomena, such as, the recirculation vortex (Cochrane, Walters *et al.* [3]), the shift of the vortex center (Grillet, Yang *et al.* [4]), *etc*., were revealed in early studies. The flow structure is affected by many factors, *e.g.* the aspect ratios (Grillet, Yang *et al.* [4]) and the height of the cavity (Grillet, Shaqfeh *et al.* [1]), the velocity, the flow rate (Kim, Öztekin *et al.* [5]) and the elastic nature of the fluid (Takehiro [6]), *etc*.

Cochrane *et al*. (Cochrane, Walters *et al.* [3]) observed the behavior of the non-Newtonian (PAC) flow and the Newtonian flow past a square cavity. The recirculating vortex inside the cavity is symmetric only for the non-Newtonian fluid under small Re and De values.

Kim *et al*. (Kim, Öztekin *et al.* [5]) investigated the flow structure of the viscoelastic fluid past a square cavity experimentally by capturing the images in the flow plane. They found that the streamline inside the cavity is symmetric at low flow rates. However, an asymmetric re-circulating flow cell occurs in the cavity and the streamlines shift deeper into the cavity at higher flow rates.

Grillet *et al*. (Grillet, Yang *et al.* [4]) simulated the effects of fluid elasticity on the flow kinematics and the stress distribution in lid driven cavity flow with finite element method. They showed the contours of the stream function for several aspect ratios of the cavity graphically. The primary recirculation vortex and the shift phenomenon of the vortex center were reported in their study.

Kim *et al*. (Kim, Öztekin *et al.* [5]) reported the critical values of the De number for the onset of cellular flow transition in a square cavity. At low De flow, the

* Corresponding author (gckuo@tiit.edu.tw)



DOI : 10.1017/jmech.2012.143
Copyright © 2013 The Society of Theoretical and Applied Mechanics, R.O.C.
https://doi.org/10.1017/jmech.2012.143 Published online by Cambridge University Press

inertialess viscoelastic flow inside the cavity is symmetric. At higher De, flow becomes asymmetric. Grillet *et al*. (Grillet, Shaqfeh *et al.* [1]) confirmed that the height of the cavity is the important length scale for determining the onset of instability in shallow cavities experimentally.

Yamamoto *et al*. (Takehiro [6]) studied three-dimensional viscoelastic flows in a rectangular channel with a cavity both numerically and experimentally. A spiral vortex appears at the center of the main recirculation zone under high Weissenberg numbers. The spiral flow behavior, which is caused by the normal stress effects, arises from the elasticity of viscoelastic fluids.

Al-Amiri (Al-Amiri, Khanafer *et al.* [7]) investigated the steady mixed convection in a square lid-driven cavity under the combined buoyancy effects of thermal and mass diffusion. The heat and mass transfer rates were examined by using several operational dimensionless parameters, *e.g.* the Richardson number, Lewis number and buoyancy ratio parameter, *etc*.

Takehiro *et al*. (Takehiro [6]) demonstrated a numerical simulation of lid-driven cavity flows by the hybrid numerical method. The vorticity contours shift further away from the cavity center as the Reynolds number increases.

The unsteady flow of a second-grade viscoelastic fluid on a backward-facing step was studied numerically (Hsu and Chou [2]). The streamline patterns and the reattachment length were compared by changing the Reynolds number and the elastic number. A transient mixed convection of a second-grade viscoelastic fluid on a backward-facing step numerically in (Hsu, Chen *et al.* [8]). The size of the primary recirculation zone increases with a higher Richardson number, but decreases with a higher elastic number.

The transient mixed convection of a second-grade viscoelastic fluid past an inclined backward facing step was studied numerically in (Kung, Hsu *et al.* [9]). The reattachment length increases to the maximum as the inclined angle increases. The reattachment length increases as the Reynolds number increases or the elastic coefficient decreases.

In this study, the cavity is considered as a combination of a backward-facing step followed by a forward-facing step. The characteristics of the flow field when the second grade viscoelastic fluid flows past a cavity in a horizontal channel are studied numerically. The continuity equation and the momentum equation are firstly converted into the vorticity and stream function equation. Both the finite difference method and the Gauss-Seidel method with successive over relaxation (SOR) are applied to the discrete equations for better convergence during the solution iterations. The relevance of the flow phenomenon caused by different fluid's elasticity and Reynolds number are studied. The height and the shape of the main recirculation zone in the cavity are compared to find the characters of the cavity flow.

## 2. MATHEMATICAL METHOD

### 2.1 Model Representation

The geometry model used for the cavity in a horizontal channel is shown in Fig. 1. The height of the backward and the forward-facing steps are both with the same height. The origin of Cartesian coordinate system is located at corner point A. The *x*-axis is along the flow direction. The height of the channel, the total length, the length of the entrance, the height of the steps and the width of the cavity are denoted as H, L, L1, S and W, respectively. The aspect ratio of the cavity is defined as $\Lambda = S/W$.

In this paper, we suggest H, the height of the steps, is the unit length, *i.e.* $H = 1$. The dimesions of the geometry model are given as: $L = 5$, $S = 0.5$ and $L1 = 0.5$. In order to compare the effects of different cavity lengths on the flow field, the values of the width of the cavity (W) is set to be 0.5, 1.0 and 1.5. Therefore, the values of the aspect ratio ($\Lambda$) are: 1, 0.5 and 0.33, respectively.

Some fundamental assumptions are used in the present study to simplify the problem:

1. Two-dimensional incompressible flow is considered.
2. The second-grade viscoelastic fluid is used,
3. The material properties of the flow, such as density, are constant,
4. A fully developed flow is assumed at the entrance.
5. The Neumann Boundary Condition is assumed along the streamline at the exit,
6. The viscous dissipation effect in the energy equation is not considered.
7. The effect of gravity is neglected.
8. No-slip condition is applied to all the solid boundaries.

### 2.2 Governing Equations

Rivlin and Ericksen (Rivlin and Ericksen [10]) presented a stress model for the homogeneous, incompressible and second grade viscoelastic fluid.

$$\mathbf{T} = -p\mathbf{I} + \mu\mathbf{A}_1 + \alpha_1\mathbf{A}_2 + \alpha_1\mathbf{A}_1^2 \tag{1}$$

where $p$ is the pressure, $\mathbf{T}$ is the stress tensor, $\mathbf{I}$ is the identity matrix, $\mu$ is the dynamic viscosity. $\alpha_1$ and $\alpha_2$ are the first and the second normal stress coefficients related to the material modulus, respectively.

The kinematical tensors $\mathbf{A}_1$ and $\mathbf{A}_2$ are defined by

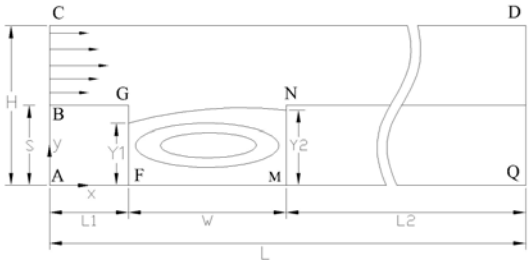



Fig. 1 Schematic of the channel with a cavity



https://doi.org/10.1017/jmech.2012.143 Published online by Cambridge University Press

$$\mathbf{A}_1 = \nabla\mathbf{V} + (\nabla\mathbf{V})^T \tag{2}$$

$$\mathbf{A}_2 = \frac{d}{dt}\mathbf{A}_1 + \mathbf{A}_1\nabla\mathbf{V} + (\nabla\mathbf{V})^T\mathbf{A}_1 \tag{3}$$

where $\mathbf{V} = (u, v)$ is the velocity vector of the flow and $d/dt$ is the material time derivative. By substituting Eq. (1) into the momentum equations, Rajagopal *et al*. [11] (Rajagopal, Gupta *et al.* [11]) showed the equations for the viscoelastic fluid.

$$\rho\frac{d}{dt}\mathbf{V} = \nabla\cdot\mathbf{T} + \rho\mathbf{b} \tag{4}$$

where $\rho$ is the density of fluid, $\mathbf{b}$ is the body force, the conservative body force is assumed to be $\mathbf{b} = \nabla\Phi$.

For the two-dimensional incompressible flow problem, the following assumptions are satisfied.

$$\nabla\cdot\mathbf{V} = 0 \tag{5}$$

$$\mathbf{P} = p - \alpha_1\mathbf{V}\cdot\nabla^2\mathbf{V} - (2\alpha_1 + \alpha_2)\,|\,\mathbf{A}_1\,|^2 + \frac{1}{2}\rho\,|\,\mathbf{V}\,|^2 + \rho\phi \tag{6}$$

We can replace $\alpha_2$ as in terms of $\alpha_1$ by using the relationships shown as Eq. (7) suggested by Fosdick and Rajagopal (Fosdick and Rajagopal [12]) in 1978.

$$\mu \geq 0\ ,\ \ \alpha_1 \geq 0\ ,\ \ \alpha_1 + \alpha_2 = 0 \tag{7}$$

The governing equations for the viscoelastic fluid can be written as

$$\frac{\partial u}{\partial x} + \frac{\partial v}{\partial y} = 0 \tag{8}$$

$$\begin{aligned}
&\frac{\partial u}{\partial t} + u\frac{\partial u}{\partial x} + v\frac{\partial u}{\partial y} \\
&= -\frac{1}{\rho}\frac{\partial P}{\partial x} + \frac{\mu}{\rho}\left(\frac{\partial^2 u}{\partial x^2} + \frac{\partial^2 u}{\partial y^2}\right) \\
&\quad + \frac{\alpha_1}{\rho}\left[\left(\frac{\partial^3 u}{\partial x^2\partial t} + \frac{\partial^3 u}{\partial y^2\partial t}\right) + 2\frac{\partial^2}{\partial x^2}\left(u\frac{\partial u}{\partial x} + v\frac{\partial u}{\partial y}\right)\right. \\
&\quad + 4\left(\frac{\partial u}{\partial x}\frac{\partial^2 u}{\partial x^2} + \frac{\partial v}{\partial x}\frac{\partial^2 v}{\partial x^2}\right) + \frac{\partial^2}{\partial x\partial y}\left(u\frac{\partial v}{\partial x} + v\frac{\partial v}{\partial y}\right) \\
&\quad \left. + \frac{\partial^2}{\partial y^2}\left(u\frac{\partial u}{\partial x} + v\frac{\partial u}{\partial y}\right) + 2\frac{\partial}{\partial y}\left(\frac{\partial u}{\partial x}\frac{\partial u}{\partial y} + \frac{\partial v}{\partial x}\frac{\partial v}{\partial y}\right)\right]
\end{aligned} \tag{9}$$

$$\begin{aligned}
&\frac{\partial u}{\partial t} + u\frac{\partial v}{\partial x} + v\frac{\partial v}{\partial y} \\
&= -\frac{1}{\rho}\frac{\partial P}{\partial y} + \frac{\mu}{\rho}\left(\frac{\partial^2 v}{\partial x^2} + \frac{\partial^2 v}{\partial y^2}\right) \\
&\quad + \frac{\alpha_1}{\rho}\left[\left(\frac{\partial^3 v}{\partial x^2\partial t} + \frac{\partial^3 v}{\partial y^2\partial t}\right) + 2\frac{\partial^2}{\partial y^2}\left(u\frac{\partial v}{\partial x} + v\frac{\partial v}{\partial y}\right)\right. \\
&\quad + 4\left(\frac{\partial u}{\partial y}\frac{\partial^2 u}{\partial y^2} + \frac{\partial v}{\partial y}\frac{\partial^2 v}{\partial y^2}\right) + \frac{\partial^2}{\partial x\partial y}\left(u\frac{\partial u}{\partial x} + v\frac{\partial u}{\partial y}\right) \\
&\quad \left. + \frac{\partial^2}{\partial x^2}\left(u\frac{\partial v}{\partial x} + v\frac{\partial v}{\partial y}\right) + 2\frac{\partial}{\partial x}\left(\frac{\partial u}{\partial x}\frac{\partial u}{\partial y} + \frac{\partial v}{\partial x}\frac{\partial v}{\partial y}\right)\right]
\end{aligned} \tag{10}$$

## 3. DIMENSIONLESS PARAMETERS

To obtain the dimensionless momentum equations, the dimensionless variables are defined as

$$X = \frac{x}{H}\ ,\ Y = \frac{y}{H} \tag{11}$$

$$U = \frac{u}{U_0}\ ,\ V = \frac{v}{U_0} \tag{12}$$

$$\tau = \frac{t}{H/U_0}\ ,\ p^* = \frac{P - P_\infty}{\rho U_0^2} \tag{13}$$

$$\mathrm{Re} = \frac{\rho U_0 H}{\mu} \tag{14}$$

$$E = \frac{\alpha_1}{\rho H^2} \tag{15}$$

where Re is the Reynolds Number, $H$ is the characteristic length, $E$ is the elasticity of the viscoelastic fluid, $U_0$ is the average speed of the flow at the entrance, $P_\infty$ is the reference pressure.

The dimensionless momentum equations are obtained by substituting the dimensionless variables into the Eqs. (8), (9) and (10).

$$\frac{\partial U}{\partial X} + \frac{\partial V}{\partial Y} = 0 \tag{16}$$

$$\begin{aligned}
&\frac{\partial U}{\partial \tau} + U\frac{\partial U}{\partial X} + V\frac{\partial U}{\partial Y} \\
&= -\frac{\partial p^*}{\partial X} + \frac{1}{\mathrm{Re}}\left(\frac{\partial^2 U}{\partial X^2} + \frac{\partial^2 U}{\partial Y^2}\right) \\
&\quad + E\left[\left(\frac{\partial^3 U}{\partial X^2\partial \tau} + \frac{\partial^3 U}{\partial Y^2\partial \tau}\right) + 2\frac{\partial^2}{\partial X^2}\left(U\frac{\partial U}{\partial X} + V\frac{\partial U}{\partial Y}\right)\right. \\
&\quad + 4\left(\frac{\partial U}{\partial X}\frac{\partial^2 U}{\partial X^2} + \frac{\partial V}{\partial X}\frac{\partial^2 V}{\partial X^2}\right) + \frac{\partial^2}{\partial X\partial Y}\left(U\frac{\partial V}{\partial X} + V\frac{\partial V}{\partial Y}\right) \\
&\quad \left. + \frac{\partial^2}{\partial Y^2}\left(U\frac{\partial U}{\partial X} + V\frac{\partial U}{\partial Y}\right) + 2\frac{\partial}{\partial Y}\left(\frac{\partial U}{\partial X}\frac{\partial U}{\partial Y} + \frac{\partial V}{\partial X}\frac{\partial V}{\partial Y}\right)\right]
\end{aligned} \tag{17}$$



https://doi.org/10.1017/jmech.2012.143 Published online by Cambridge University Press

$$\frac{\partial V}{\partial \tau}+U\frac{\partial V}{\partial X}+V\frac{\partial V}{\partial Y}$$
$$=-\frac{\partial p^*}{\partial Y}+\frac{1}{\mathrm{Re}}\left(\frac{\partial^2 V}{\partial X^2}+\frac{\partial^2 V}{\partial Y^2}\right)$$
$$+E\left[\left(\frac{\partial^3 V}{\partial X^2\partial \tau}+\frac{\partial^3 V}{\partial Y^2\partial \tau}\right)+2\frac{\partial^2}{\partial Y^2}\left(U\frac{\partial V}{\partial X}+V\frac{\partial V}{\partial Y}\right)\right.$$
$$+4\left(\frac{\partial U}{\partial Y}\frac{\partial^2 U}{\partial Y^2}+\frac{\partial V}{\partial Y}\frac{\partial^2 V}{\partial Y^2}\right)+\frac{\partial^2}{\partial X\partial Y}\left(U\frac{\partial U}{\partial X}+V\frac{\partial U}{\partial Y}\right)$$
$$\left.+\frac{\partial^2}{\partial X^2}\left(U\frac{\partial V}{\partial X}+V\frac{\partial V}{\partial Y}\right)+2\frac{\partial}{\partial X}\left(\frac{\partial U}{\partial X}\frac{\partial U}{\partial Y}+\frac{\partial V}{\partial X}\frac{\partial V}{\partial Y}\right)\right] \tag{18}$$

## 4. STREAM-VORTICITY EQUATIONS

Takehiro *et al*. (Takehiro [6]) expressed the Navier–Stokes equations in terms of stream function and vorticity. The vorticity is defined by

$$\vec{\omega}=\nabla\times\vec{V} \tag{19}$$

The advantages of the stream-vorticity equation are: (1) It automatically satisfies continuity; (2) In the process of dimensionless variable transformation, boundary conditions are not required for the pressure variable. The vorticity function (ω) and the stream function (ψ) are introduced to replace the velocity and pressure variables in the governing Eqs. (16) ~ (18). For two dimensional Cartesian coordinate, the vorticity function is defined as

$$\omega=\frac{\partial V}{\partial X}-\frac{\partial U}{\partial Y} \tag{20}$$

The stream function is defined as

$$\frac{\partial \psi}{\partial Y}=U$$
$$-\frac{\partial \psi}{\partial X}=V \tag{21}$$

To eliminate the pressure terms in Eqs. (17) and (18), we use

$$\frac{\partial}{\partial X}Eqn.(18)-\frac{\partial}{\partial Y}Eqn.(17) \tag{22}$$

After some manipulations similar to our early study (Hsu, Chen *et al.* [8]), the dimensionless stream-vorticity equation can be written as

$$\frac{\partial \omega}{\partial \tau}+\frac{\partial(\mathrm{U}\omega)}{\partial \mathrm{X}}+\frac{\partial(\mathrm{V}\omega)}{\partial \mathrm{Y}}=\frac{1}{\mathrm{Re}}\left(\frac{\partial^2\omega}{\partial \mathrm{X}^2}+\frac{\partial^2\omega}{\partial \mathrm{Y}^2}\right)$$
$$+\mathrm{E}\left[\frac{\partial}{\partial\tau}\left(\frac{\partial^2\omega}{\partial \mathrm{X}^2}+\frac{\partial^2\omega}{\partial \mathrm{Y}^2}\right)+\left(\frac{\partial^3\phi}{\partial \mathrm{X}^2\partial Y}\frac{\partial\omega}{\partial X}+\frac{\partial\phi}{\partial Y}\frac{\partial^3\omega}{\partial X^3}\right.\right.$$
$$-\frac{\partial^3\omega}{\partial \mathrm{X}^2\partial Y}\frac{\partial\phi}{\partial X}+\frac{\partial\omega}{\partial Y}\frac{\partial^3\phi}{\partial X^3}\Big)+\left(\frac{\partial^3\phi}{\partial \mathrm{Y}^2}\frac{\partial\omega}{\partial X}+\frac{\partial\phi}{\partial Y}\frac{\partial^3\omega}{\partial Y^2\partial X}\right.$$
$$-\frac{\partial^3\omega}{\partial \mathrm{Y}^3}\frac{\partial\phi}{\partial X}-\frac{\partial\omega}{\partial Y}\frac{\partial^3\phi}{\partial Y^2\partial X}\Big)+4\left(\frac{\partial^3\omega}{\partial \mathrm{X}\partial \mathrm{Y}^2}\frac{\partial^3\phi}{\partial \mathrm{Y}^3}+\frac{\partial^2\phi}{\partial \mathrm{Y}^2}\frac{\partial^4\phi}{\partial \mathrm{X}\partial \mathrm{Y}^3}\right.$$
$$-\frac{\partial^3\phi}{\partial \mathrm{X}^2\partial \mathrm{Y}}\frac{\partial^3\phi}{\partial \mathrm{X}^3}-\frac{\partial^2\phi}{\partial \mathrm{X}^2}\frac{\partial^4\phi}{\partial \mathrm{X}^3\partial \mathrm{Y}}\Big)+2\left(\frac{\partial^2\phi}{\partial X\partial \mathrm{Y}}\frac{\partial^4\phi}{\partial X^4}\right.$$
$$\left.\left.-\frac{\partial^2\phi}{\partial X\partial Y}\frac{\partial^4\phi}{\partial Y^4}-\omega\frac{\partial^4\phi}{\partial X^3\partial Y}-\omega\frac{\partial^4\phi}{\partial X\partial Y^3}\right)\right] \tag{23}$$

By substituting Eq. (21) into Eq. (20), an equation by the combination of ω and ψ is obtained.

$$\frac{\partial^2\psi}{\partial X^2}+\frac{\partial^2\psi}{\partial Y^2}=-\omega \tag{24}$$

The boundary conditions are shown as below:

1. Due to assumption (4), a fully-developed flow is assumed at the entrance.

$$U=U(Y)=-48(Y-0.5)^2+24(Y-0.5)$$

$$\psi=\int_{0.5}^{1}UdY=-16(Y-0.5)^3+12(Y-0.5)^2$$

2. Due to assumption (5), the Neumann Boundary Condition is assumed on the exit:

$$\frac{\partial \mathrm{U}}{\partial \mathrm{X}}=\frac{\partial \mathrm{V}}{\partial \mathrm{X}}=0\ ,\quad \frac{\partial\varphi}{\partial \mathrm{X}}=0\ ,\quad \frac{\partial\omega}{\partial \mathrm{X}}=0$$

3. Due to assumption (8), No Slip Condition is used on all the solid boundaries.

$$U=V=0$$

$\psi=1$, on the upper plate.

$\psi=0$, on the lower plate.

## 5. FINITE DIFFERENCE EQUATIONS

The finite difference equation is obtained from Eq. (23) with implicit upwind difference method. The finite difference equation can be written as:



https://doi.org/10.1017/jmech.2012.143 Published online by Cambridge University Press

$$\omega_{i,j,n+1}^{k+1} = (1-s)\omega_{i,j,n+1}^{k} + s\left\{\omega_{i,j,n} + \frac{\Delta\tau}{\mathrm{Re}}\left[\frac{1}{(\Delta X)^2}(\omega_{i-1,j,n+1}^{k} + \omega_{i+1,j,n+1}^{k}) + \frac{1}{(\Delta Y)^2}(\omega_{i,j-1,n+1}^{k} + \omega_{i,j+1,n+1}^{k})\right] - \frac{\Delta\tau}{\Delta X}\left[(U\omega)_{i+1/2,j,n+1}^{k} - (U\omega)_{i-1/2,j,n+1}^{k}\right] - \frac{\Delta\tau}{\Delta Y}\left[(V\omega)_{i,j+1/2,n+1}^{k} - (V\omega)_{i,j-1/2,n+1}^{k}\right] + \Delta\tau E S_0\right\} \Bigg/ \left[1 + \frac{\Delta\tau}{\mathrm{Re}}\left(\frac{2}{(\Delta X)^2} + \frac{2}{(\Delta Y)^2}\right)\right] \quad (25)$$

where $s$ is the relaxation factor for the stream-vorticity equations. $E$ is the elasticity of the fluid. $S_0$ is the source term including the terms of third and fourth differential items. $f_{i+1/2,j}$ represents the average of $f_{i,j}$ and $f_{i+1,j}$. Where $f$ represents $U$, $V$ or $\omega$.

The line-Gauss–Seidel (LGS) and alternative direction implicit (ADI) methods are applied to solve the stream-vorticity equation. The stream function combined with the Gauss–Seidel method is shown as below:

$$\begin{aligned}\psi_{i,j}^{(k+1)} &= \psi^{(k)} + \lambda\left\{\psi_{i,j}^{(k+1)*} - \psi_{i,j}^{(k)}\right\} \\ &= \lambda c_1\left[\psi_{i-1,j}^{(k+1)*} + \psi_{i+1,j}^{(k)}\right] \\ &\quad + \lambda c_2\left[\psi_{i,j-1}^{(k+1)*} + \psi_{i,j+1}^{(k)}\right] \\ &\quad + \lambda c_1 c_3 \omega_{i,j} - (\lambda - 1)\varphi_{i,j}^{(k)}\end{aligned} \quad (26)$$

where $\psi_{i,j}^{(k+1)}$ is the $(k+1)$ th iteration value by the Gauss–Seidel method with over-relaxation,

$\psi_{i,j}^{(k+1)*}$ is $(k+1)$ the th iteration value by the Gauss–Seidel method with over-relaxation,

$\psi_{i,j}^{(k)}$ is the $(k)$ th iteration value by the Gauss–Seidel method with over-relaxation,

$$c_1 = \frac{(\Delta Y)^2}{2\left[(\Delta X)^2 + (\Delta Y)^2\right]},\quad c_2 = \frac{(\Delta X)^2}{2\left[(\Delta X)^2 + (\Delta Y)^2\right]},\quad c_3 = (\Delta X)^2$$

The under-relaxation factor $s$ is introduced into the stream-vorticity equations. The over-relaxation factor $\lambda$ is used in stream function. The modulation of $s$ and $\lambda$ can avoid the divergence and accelerate the convergence of numerical scheme of the non-linear equations.

## 6. BOUNDARY CONDITIONS

According the assumption 8, no-slip condition is used on all the solid boundaries, *i.e.* $U = V = 0$. The stream functions of the horizontal surface and the surfaces of the cavity all are $\psi = 0$, and that of the top surface is $\psi = 1$.

According the assumption 4, a fully-developed flow is assumed at the entrance. The initial value of the vorticity of the flow field is assumed as zero. Other boundary conditions are defined as:

(a) Top surface (C-D in Fig. 1):

$$\omega_{i,N} = -\frac{\partial^2\psi}{\partial Y^2} = \frac{2(\psi_{i,N} - \psi_{i,N\text{-}1})}{\Delta Y^2} \quad (27)$$

(b) Horizontal surface of step and bottom surface of the cavity (B-G, F-M and N-Q in Fig. 1):

$$\omega_{i,1} = -\frac{\partial^2\psi}{\partial Y^2} = \frac{2(\psi_{i,1} - \psi_{i,2})}{\Delta Y^2} \quad (28)$$

(c) Left vertical surface of the cavity (F-G in Fig. 1)

$$\omega = -\frac{\partial^2\psi}{\partial X^2} = \frac{2(\psi_{I,j} - \psi_{I+1,j})}{\Delta X^2} \quad (29)$$

(d) Right vertical surface of the cavity (M-N in Fig. 1)

$$\omega = -\frac{\partial^2\psi}{\partial X^2} = \frac{2(\psi_{I,j} - \psi_{I-1,j})}{\Delta X^2} \quad (30)$$

(e) Top corner of step (points G and N in Fig. 1):

$$\omega_{i,j} = \frac{-1}{(\Delta X)^2}(\psi_{i+1,j} - \psi_{i,j}) + \frac{-1}{(\Delta Y)^2}(\psi_{i,j+1} - \psi_{i,j}) \quad (31)$$

(f) Bottom corner of step (points F and M in Fig. 1):

$$\omega = 0 \quad (32)$$

(g) Vorticity and stream function at exit plane (D-Q in Fig. 1)

$$f_{I,j} = f_{I-4,j} - 2f_{I-3,j} + 2f_{I-1,j} \quad (33)$$

where $f$ represents $\omega$, or $\psi$.

## 7. NUMERICAL SOLUTION PROCEDURES

The procedures to solve the difference Equations numerically are shown as below:

1. Set the initial value of the vorticity, stream function, the velocity vectors and the boundary conditions.
2. Solve the stream-vorticity equations to obtain the value of the vorticity and the stream function.
3. Calculate the horizontal and vertical components of the velocity vector from the stream function.
4. Calculate the vorticity on the boundary from the stream function and the vorticity.
5. Iterate the steps (2) to step (4) until the criterion of convergence is satisfied.
6. Iterate the steps (2) to step (5) until the criterion of convergence for the steady state is satisfied.



https://doi.org/10.1017/jmech.2012.143 Published online by Cambridge University Press

The parameter settings of the relaxation factor, the time step, and the entrance length are 0.2, 0.001, and 0.5. The relaxation factor is set as 0.1 for some high Reynolds number or high coefficient of elasticity cases. The range of Reynolds number is set as [10,400] with an incremental value 10. The elasticity coefficient is set as the range from 0.0005 to 0.001 with an incremental value 0.0001.

The convergent solution is obtained during numerical iteration at each time step. Some shooting values are assumed for the non-linear terms in the vorticity equation at the beginning of the iteration. They are renewed within each time step. The criterion of convergence for each time interval is

$$\frac{|f_{i,j,n}^{k+1} - f_{i,j,n}^{k}|}{|\mathrm{Max}(f^{k})|} \le 1\times10^{-6} \tag{34}$$

The criterion of convergence for the flow reaching the steady state is

$$\frac{|f_{i,j,n+1}^{k} - f_{i,j,n}^{k}|}{|\mathrm{Max}(f_{n+1})|} \le 1\times10^{-5} \tag{35}$$

where $f$ represents ω, or ψ. $k$ is the number of iteration during the time step and $n$ is the time marching index. Max($f^k$) is the maximum value of space domain during the kth iteration and Max($f_{n+1}$) is the maximum value of space domain during the whole iteration time.

## 8. GRID QUALITY TESTING

A uniform grid system is applied to the present work. The accuracy of the solution is poor for too sparse grid system. However, too much computing time will waste for too dense grid system. Therefore, an evaluation about the quality of the grid system is necessary.

Four grid systems, such as 289 × 17, 577 × 33, 1153 × 65 and 1729 × 97 are used in this assessment. The convergence trend of stream function (ψ) and vorticity (ω) according these grid systems are compared in Figs. 2 and 3, respectively.

Test results show that the difference of the convergence values decreases by using denser grid system for both stream function and vorticity curves. The convergence values between 1153 × 65 grid sytem and 1729 × 97 grid sytem are very close each other. Therefore, the system with 1153 × 65 grids was chosen as the better grid system for a balance between the solution accuracy and the computing time.

## 9. RESULTS AND DISCUSSION

### 9.1 Contours of the Streamlines in the Cavity

Figure 4 shows the contours of streamlines for the fluid with elasticity $E$ = 0.0005 past the cavity with aspect ratio Λ = 0.5 as $W = H$. Figure 6 shows the contours of streamlines for the fluid with elasticity $E$ = 0.001 past the same cavity.

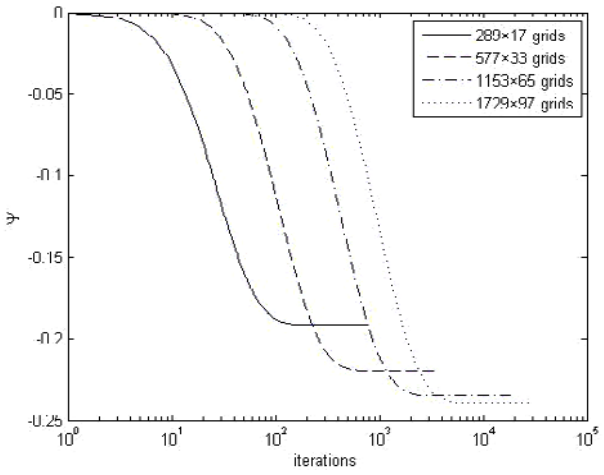



Fig. 2 Convergence trend of streamline fnction (ψ) at the mid-point in the cavity

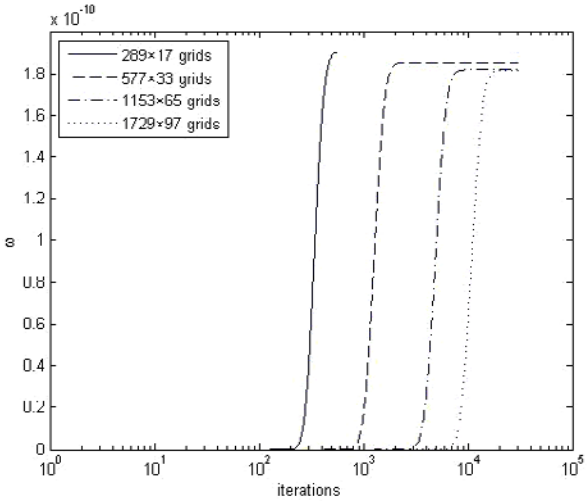



Fig. 3 Convergence trend of vorticity (ω) at the mid-point in the cavity

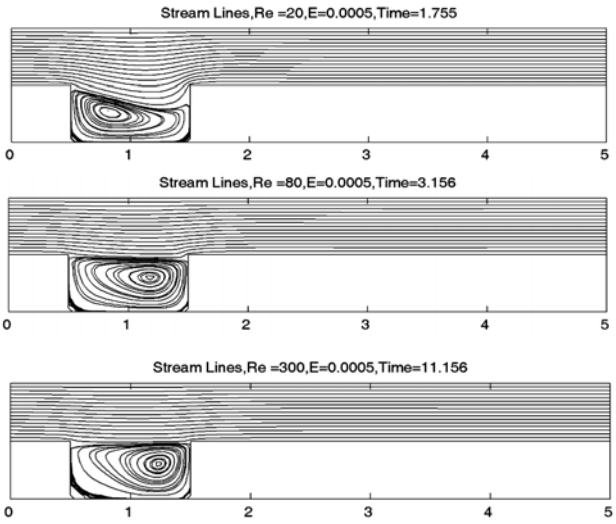



Fig. 4 Contours of streamlines in the channel with a Λ = 0.5 cavity as $E$ = 0.0005



https://doi.org/10.1017/jmech.2012.143 Published online by Cambridge University Press

The recirculation zone appears in the region of the cavity. The vortex center is close to the backward-facing step at low Reynolds number, such as Re = 20. However, it is close to the forward-facing step when the Reynolds number exceeds 80. The vortex center drifts downstream in the cavity as the Reynolds number increases. This result is agree with the study of Grillet *et al*. [4] (Grillet, Yang *et al.* [4]).

### 9.2 Flow Patterns in the Cavity

By observing the contours of streamlines in Figs. 4 and 6, the slope of streamline changes with the changing of the shape of the recirculation zone. For the convenience to discuss the slope of streamline, the symbol Y1 is defined as the height measured from the bottom of the step to the dividing streamline near the backward step. Similarly, the symbol Y2 is defined as the height measured from the bottom of the step to the dividing streamline near the forward step. In this paper, the flow patterns are represented as the first flow, the transition flow and the second flow for Y1 > Y2, Y1 = Y2 and Y1 < Y2, respectively.

Figure 4 shows that Y1 is larger than Y2 as Reynolds number is 20; however, Y1 is less than Y2 as Reynolds number is 300. The first flow appears in the cavity as Re = 20; however, the second flow appears in the cavity as Re = 300. We speculate that the transition flow will appear in the cavity while the values of Y1 and Y2 equal to each other.

Figure 5 shows the trends of the height of recirculation zone Y1 and Y2 curves. The curves Y1 and Y2 intersect each other at point P where Y1 = Y2 = 0.470843 and Re = 147.839. The transitional flow appears in the cavity with aspect ratio $\Lambda = 0.5$ at Re = 147.839 as the fluid with elasticity $E = 0.0005$.

### 9.3 Effects of Fluid Elasticity

Figure 6 shows the contours of stream function for the fluid with elasticity $E = 0.001$ past cavity with aspect ratio $\Lambda = 0.5$. Reynolds number is ranged from $20 \le \text{Re} \le 160$. The contours of the streamline of $E = 0.0005$and $E = 0.001$ are very similar each other at low Reynolds numbers such as Re = 20. However, they are quite different at high Reynolds numbers. The height of recirculation zone near the backward step decreases as the fluid elasticity increases from $E = 0.0005$ to $E = 0.001$.

This is consistent with the result of Cochrane *et al*. (Cochrane, Walters *et al.* [3]), which revealed that the re-circulating vortex inside the cavity is symmetric only when both Re and De are very small for the non-Newtonian fluid, but at higher flow rates the flow becomes asymmetric. It is also consistent with the result of Kim *et al*. (Kim, Öztekin *et al.* [5]), which revealed that the dividing streamline becomes asymmetric at higher flow rates, and it shifts deeper into the cavity.

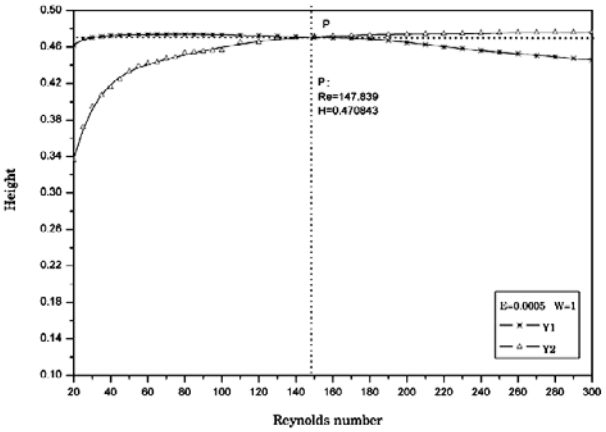



Fig. 5 Effect of Reynolds number on height of recirculation zone *Y*1 and *Y*2 as fluid with elastic coefficient $E = 0.0005$ pass through the $\Lambda = 0.5$ cavity

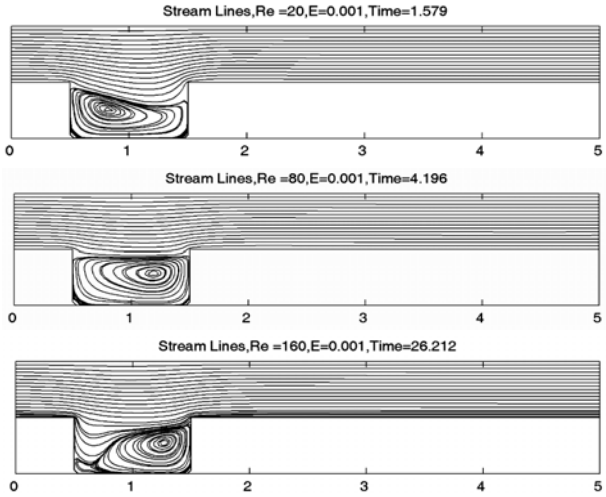



Fig. 6 Contours of streamlines in the channel with a $\Lambda = 0.5$ cavity as $E = 0.001$

Figure 7 shows the trends of Y1 and Y2 for the fluid with elasticity $E = 0.001$ past the cavity with aspect ratio $\Lambda = 0.5$. The curves Y1 and Y2 intersect each other at point P where Y1 = Y2 = 0.439224 and Re = 65.1868. We predict that the transitional flow pattern appear at Re = 65.1868 for $E = 0.001$ and $\Lambda = 0.5$.

The trends of Y2 shown in Figs. 5 and 7 are similar each other. However, the trends of Y1 are quite different: (1) the height of the transitional flow recirculation zone reduces from 0.470843 to 0.439224 as the fluid elasticity increases from to $E = 0.001$. (2) While the second flow developing from Re = 147.39 till Re = 300, the value of Y1 reduces slightly for $E = 0.0005$. The value of Y1 reduces from 0.439224 to 0.14, while Reynolds number increasing from 65.1868 to 160. Therefore, the streamlines will probe deeply into the cavity near the backward step as high elasticity fluid past the channel with a cavity at high Reynolds number.

Figure 8 shows the height difference curves for the square cavity with unity aspect ratio, that is, $\Lambda = 1$. The flow patern is predicted as the first, transitional, or the second flow pattern while the value of Y1−Y2 is positive, zero and negative.



https://doi.org/10.1017/jmech.2012.143 Published online by Cambridge University Press

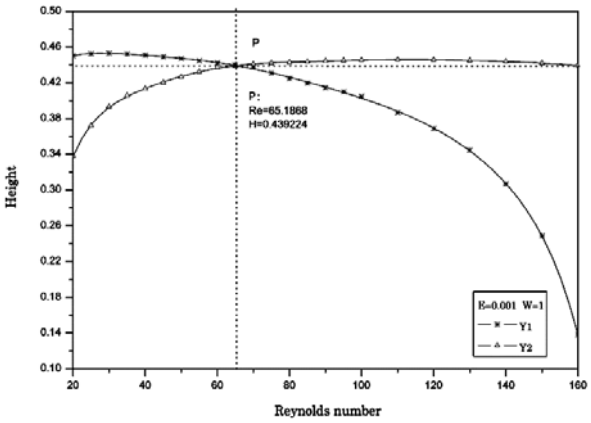



Fig. 7 Effect of Reynolds number on height of recirculation zone $Y1$ and $Y2$ as fluid with elastic coefficient $E = 0.001$ pass through the $\Lambda = 0.5$ cavity

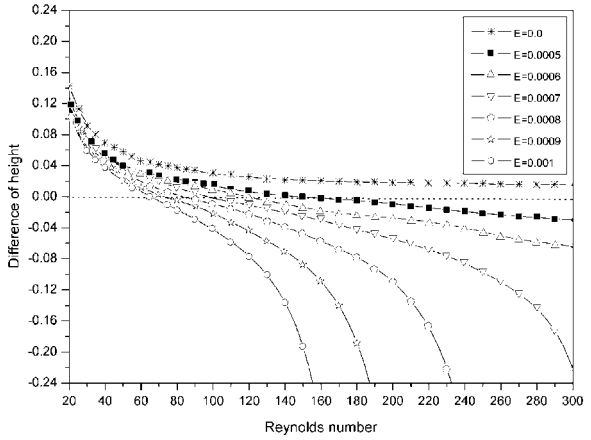



Fig. 8 Effect of Reynolds number and elastic coefficient ($E$) on height difference ($Y1$-$Y2$) in $\Lambda = 0.5$ cavity

The fluid with elasticity $E = 0$ is known as Newtonian fluid. For the Newtonian fluid, the value of Y1−Y2 reduces gradually from 0.14 to a positive value when Reynolds number increases from 20 to 300. However, for the viscoelastic fluids, the values of Y1−Y2 reduced to negative values. The values of Y1−Y2 are positive for Newtonian fluid. Therefore, the flow field inside the cavity keeps only the first flow pattern as the Newtonian fluid past the cavity.

The re-circulating flow cells are formed in the cavity along the neutral direction for flow rates beyond the critical value for the onset of elastic flow transition (Kim, Öztekin *et al.* [5]).

The transitional flow, defined as Y1 = Y2 in this paper, appears for all the viscoelastic fluids with $E > 0.0005$. Because the Y1−Y2 curve declines with more precipitous slop, the transitional flow pattern appears at lower Reynolds number for fluids with higher elasticity fluids.

Followed by the advent of the transitional flow, the second type flow, defined as Y1 < Y2, appears when Reynolds number becomes larger than that of the transitional flow. The slope of Y1−Y2 deepens when the elasticity increases in the range of $0.0007 < E < 0.001$ and $80 < \mathrm{Re} < 300$.

### 9.4 Effects of Cavity Aspect Ratio

Figure 9 shows the comparison of Reynolds number of the transitional flow pattern as six viscoelastic fluids past the cavities with aspect ratio values 1, 0.5 and 0.33. The transitional flow pattern appears at lower Reynolds number by increasing the fluid elasticity and aspect ratio of the cavity.

Figure 10 shows the variation of height of dividing streamline near backward step (Y1) with various elastic coefficient fluid pass through $\Lambda = 1(W = 0.5\mathrm{H})$, $\Lambda = 0.5(W = \mathrm{H})$ and $\Lambda = 0.33(W = 1.5\mathrm{H})$ cavities, respectively. The height of recirculation zone decreases by increasing the elasticity of the fluid. However, it increases by increasing the aspect ratio of the cavity.

## 10. CONCLUSIONS

In this paper, the flow patterns of a second grade viscoelastic fluid past a cavity in a horizontal channel are simulated numerically. The recirculation zone appears in the region of the cavity. The vortex center drifts downstream in the cavity as the Reynolds number increases. The height of recirculation zone decreases by increasing the elasticity of the fluid. However, it increases by increasing the aspect ratio of the cavity. These results are consistent with the result of early studies.

The result also reveals that the behavior of viscoelastic fluids is quite different from that of the Newtonian fluid. For viscoelastic fluids, three kinds of flow patterns appear in the sequence of the first flow pattern, the transitional flow pattern and the second flow pattern by increasing Reynolds number from 20 to 300. However, only the first flow pattern appears in Newtonian fluid flow field. The flow field is affected by the fluid elasticity as well as the aspect ratio of the cavity. The transitional flow pattern appears at lower Reynolds number as the higher elasticity fluid past the cavity with larger aspect ratio.

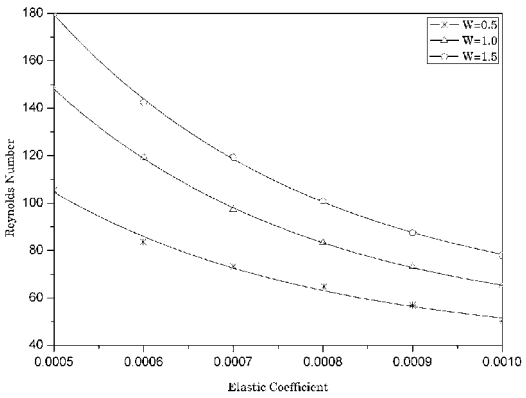



Fig. 9 Variation of Reynolds number with elastic cofficient as the transitional flow pattern occurs in $\Lambda = 1$ ($W = 0.5$), $\Lambda = 0.5$ ($W = 1.0$) and $\Lambda = 0.33$ ($W = 1.5$) cavities



https://doi.org/10.1017/jmech.2012.143 Published online by Cambridge University Press

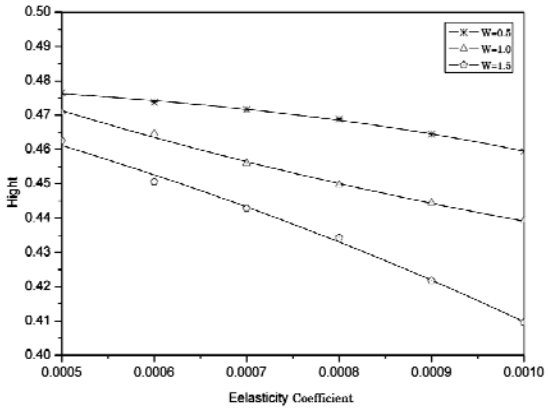



Fig. 10 Variation of height of dividing streamline near backward step ($Y1$) with various elastic coefficient in $\Lambda = 1$ ($W = 0.5$), $\Lambda = 0.5$ ($W = 1.0$) and $\Lambda = 0.33$ ($W = 1.5$) cavities

## NOMENCLATURES

| | |
|---|---|
| $\mathbf{A}_1$ | kinematical tensor |
| $\mathbf{A}_2$ | kinematical tensor |
| $\mathbf{b}$ | body force |
| $E$ | elasticity of fluid |
| $H$ | height of channel |
| $\mathbf{I}$ | identity matrix |
| L | length of channel |
| L1 | length of entrance |
| $P$ | pressure |
| $P_\infty$ | reference pressure |
| Re | Reynolds number |
| $s$ | relaxation factor for the stream-vorticity equation |
| $S$ | height of cavity |
| $S_0$ | source term |
| $t$ | time |
| $\mathbf{T}$ | stress tensor |
| $u$ | horizontal flow velocity |
| $U$ | dimensionless horizontal velocity |
| $U_0$ | average flow speed at entrance |
| $v$ | vertical flow velocity |
| $\mathbf{V}$ | flow velocity vector |
| W | width of cavity |
| $x$ | horizontal coordinate |
| $X$ | dimensionless horizontal coordinate |
| $y$ | vertical coordinate |
| $Y$ | dimensionless vertical coordinate |
| Y1 | height of dividing streamline near backward step |
| Y2 | height of dividing streamline near forward step |
| $\alpha_1$ | first normal stress coefficient |
| $\alpha_2$ | second normal stress coefficient |
| $\Lambda$ | aspect ratio of cavity |
| $\mu$ | dynamic viscosity |
| $\psi$ | stream function |
| $\omega$ | vorticity |
| $\tau$ | dimensionless time |
| $\rho$ | density of fluid |


## ACKNOWLEDGEMENT

This research was supported by the TIIT Teacher Research Support Scheme 099P-039.


## REFERENCES


1. Grillet, A. M., Shaqfeh, E. S. G. and Khomamib, B., "ObservaTions of Elastic Instabilities in Lid-Driven Cavity Flow," *Journal of Non-Newtonian Fluid Mechanics*, **94**, pp. 15–35 (2000).
2. Hsu, C. H. and Chou, T. Y., "Unsteady Flow of a Second-Grade Fluid Past a Backward-facing Step," *International Journal of Non-Linear Mechanics*, **32**, pp. 947–960 (1997).
3. Cochrane, T., Walters, K. and Webster, M. F., "On Newtonian and Non-Newtonian Flow in Complex Geometries," *Philosophical Transactions of the Royal Society A: Physical, Mathematical and Engineering Sciences*, **301**, pp. 163–181 (1981).
4. Grillet, A. M., Yang, B. and Shaqfeh, E. S. G., "Modeling of Viscoelastic Lid Driven Cavity Flow Using Finite Element Simulations," *Journal of Non-Newtonian Fluid Mechanics*, **88**, pp. 99–131 (1999).
5. Kim, J.-H., Öztekin, A. and Neti, S., "Instabilities in Viscoelastic Flow Past a Square Cavity," *Journal of Non-Newtonian Fluid Mechanics*, **90**, pp. 261–281 (2000).
6. Takehiro, Y., "Three-Dimensional Viscoelastic Flows Through a Rectangular Channel with a Cavity," *Journal of Non-Newtonian Fluid Mechanics*, **114**, pp. 13–31 (2003).
7. Al-Amiri, A. M., Khanafer, K. M. and Pop, I., "Nu-Merical Simulation of Combined Thermal and Mass Transport in a Square Lid-Driven Cavity," *International Journal of Thermal Sciences*, **46**, pp. 662–671 (2007).
8. Hsu, C. H., Chang, Y.-P. and Chen, B.-C., "Transient Mixed Convection of a Second-Grade Fluid Past a Backward-Facing Step," *International Journal of Non-Linear Mechanics*, **34**, pp. 881–893 (1999).
9. Kung, K. Y., Hsu, C. H. and Chiang, H. L., "Transient Mixed Convection Flow of a Second Grade Viscoelastic Fluid Past an Inclined Backward Facing Step," *International Journal of Non-Linear Mechanics*, **39**, pp. 427–439 (2004).
10. Rivlin, R. S. and Ericksen, J. L., "Stress Deforma-Tion Relation for Isotropic Materials," *Journal of Rational Mechanics and Analysis*, **4**, pp. 323–425 (1955).
11. Rajagopal, K. R., Gupta, A. S. and Wineman, A. S., "On a Boundary Layer Theory for Non-Newtonian Fluids," *International Journal of Engineering Science*, **18**, pp. 875–883 (1980).
12. Fosdick, R. L. and Rajagopal, K. R., "Uniqueness and Drag for Fluids of Second Grade in Steady Motion," *International Journal of Non-Linear Mechanics*, **13**, pp. 131–137 (1978).



(Manuscript received February 20, 2012, accepted for publication July 10, 2012.)





https://doi.org/10.1017/jmech.2012.143 Published online by Cambridge University Press